Supplementary Figure S1

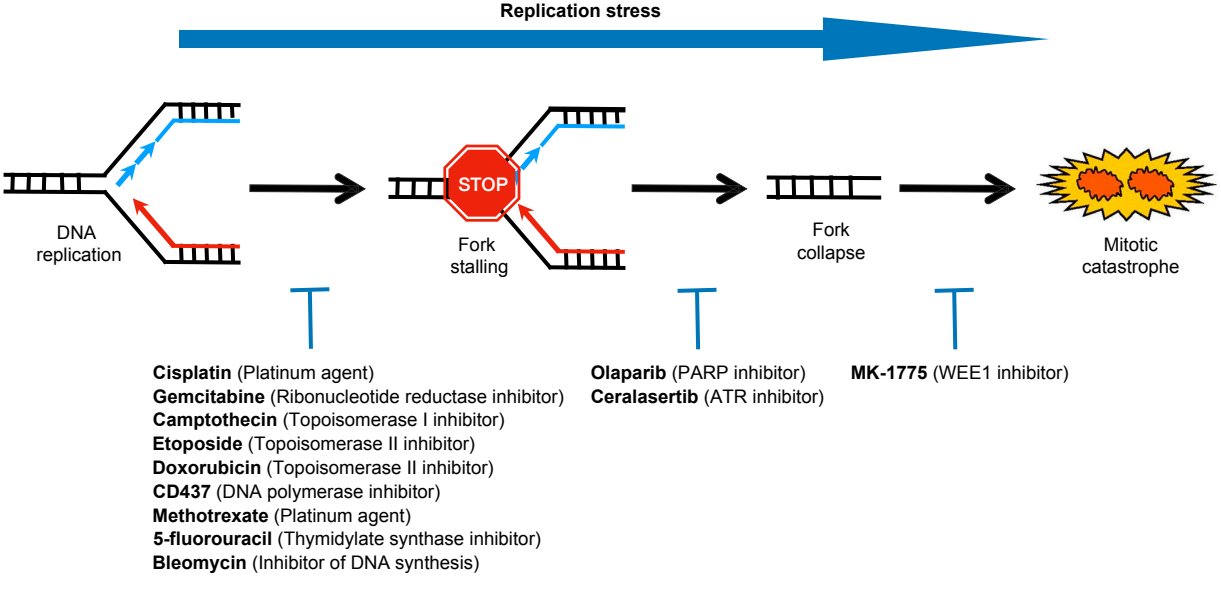

Supplementary Figure S1. Aspects of replication stress addressed by cancer therapeutics. Cancer therapeutics can invoke diverse mechanisms to induce RS. Shown are nine conventional chemotherapeutics disrupting DNA integrity or replication (left), along with three inhibitors targeting DNA damage repair signaling cascades (middle and right).

Supplementary Figure S2

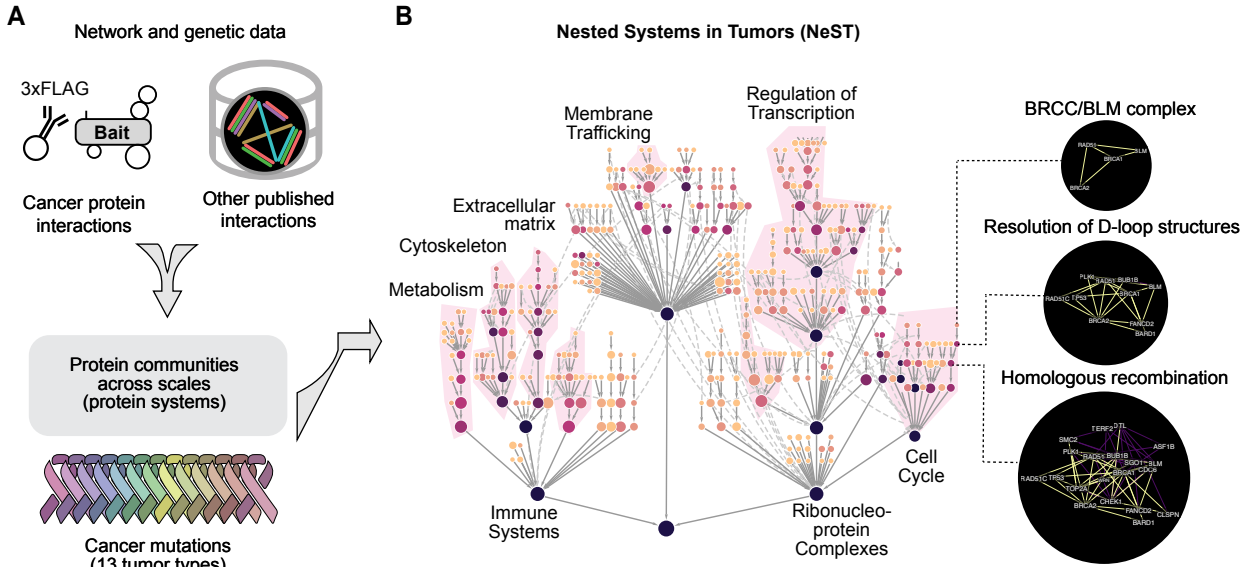

Supplementary Figure S2. Nested systems in tumors (NeST).
A, Workflow depicting construction of the NST hierarchy of protein assemblies in tumor cells. AP-MS data from 61 cancer protein baits were integrated with a compendium of published protein interaction data to produce an integrated protein network. **B,** Community detection identified nested protein assemblies inside the network. Protein assemblies under mutational selection pressure were identified, producing the NeST hierarchical map.

Supplementary Figure S3

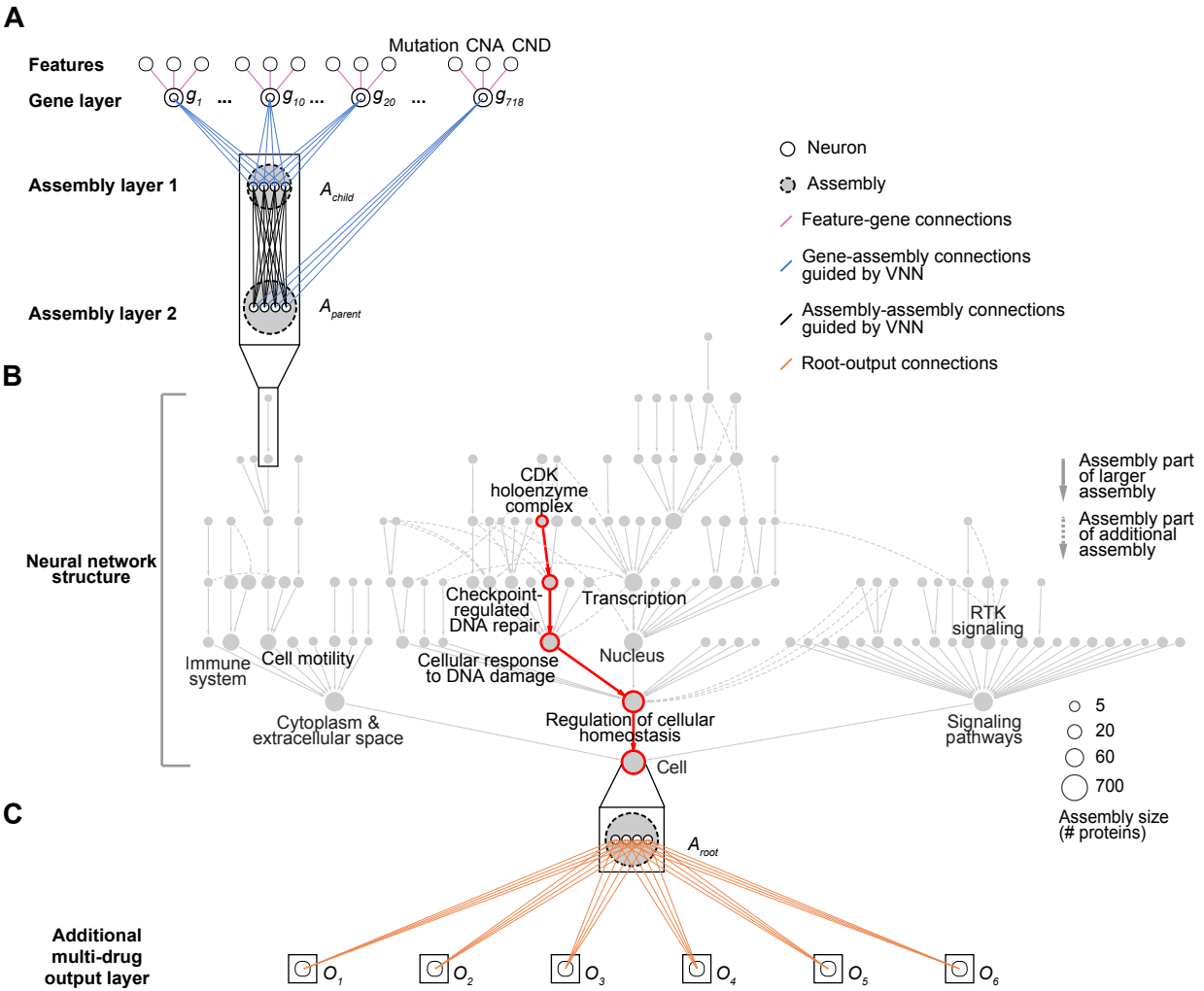

Supplementary Figure S3. VNN schematic.
A, The first layer of a VNN incorporates gene-level features, including gene mutations, copy number amplifications (CNA), and copy number deletions (CND). Subsequent layers aggregate gene-level features into assembly-level information, guided by the hierarchical relationships defined by the NeST map. The output state of each gene (*g*) and assembly (*A*) is represented by artificial neurons (one neuron per gene, multiple neurons per assembly). Hierarchical gene-to-assembly and assembly-to-assembly connections are assigned weights that are optimized during neural network training. **B,** Position of the assemblies detailed in panel (A) within the greater NeST map. Each node indicates a protein assembly. An example path of information flow, from the neurons of CDK holoenzyme complex to Cell cycle through to model Root, is shown in red. **C,** The additional layer in the multi-task (multi-drug) model enables a single model to be trained for multiple related agents by transforming the state of the Root into multiple outputs, one for each drug of interest. Apart from this final layer, all neural network weights are shared across drugs, yielding potential boosts in predictive power and model interpretation.

Supplementary Figure S4

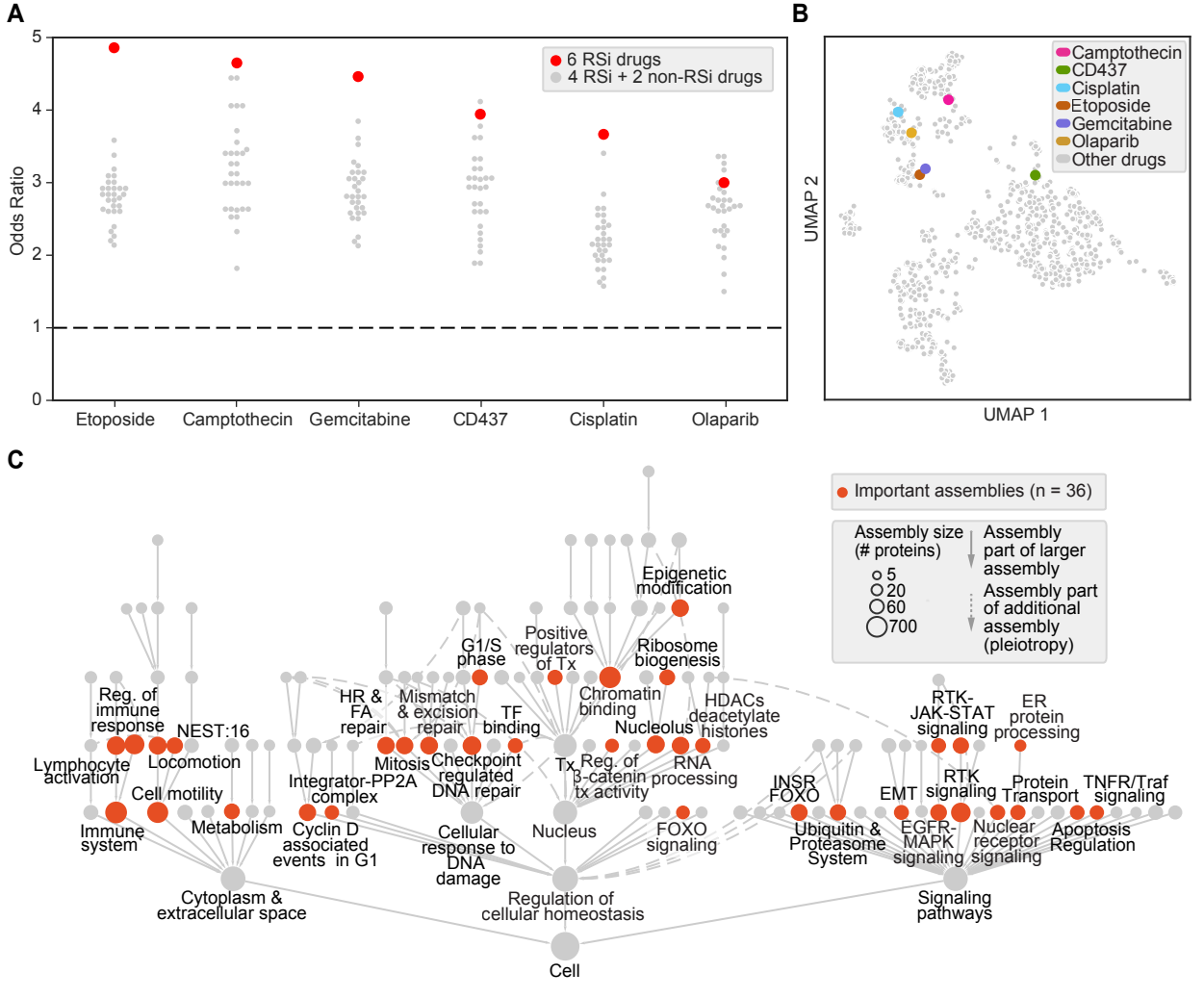

Supplementary Figure S4. Performance and interpretation of the multi-drug VNN.
A, Accuracy of the multi-drug VNN (odds ratio, y-axis) in predicting the cellular response to each of six RSi drugs (x-axis). The multi-drug VNN trained on six RSi drugs (red points) is compared to alternate multi-drug VNNs trained on combinations of RSi and non-RSi drugs (gray points). **B,** UMAP projection of drugs based on the response profiles across cell lines profiled in GDSC and CTRP. Note that all RSi drugs, save for CD437, cluster in the top left quadrant, indicating similarity in their response profiles across cell lines, with gemcitabine and etoposide showing particularly high similarity. **C,** System importance (SI) profile for the unified multi-drug VNN. The number of important assemblies is indicated in parentheses for multi-drug model.

Supplementary Figure S5

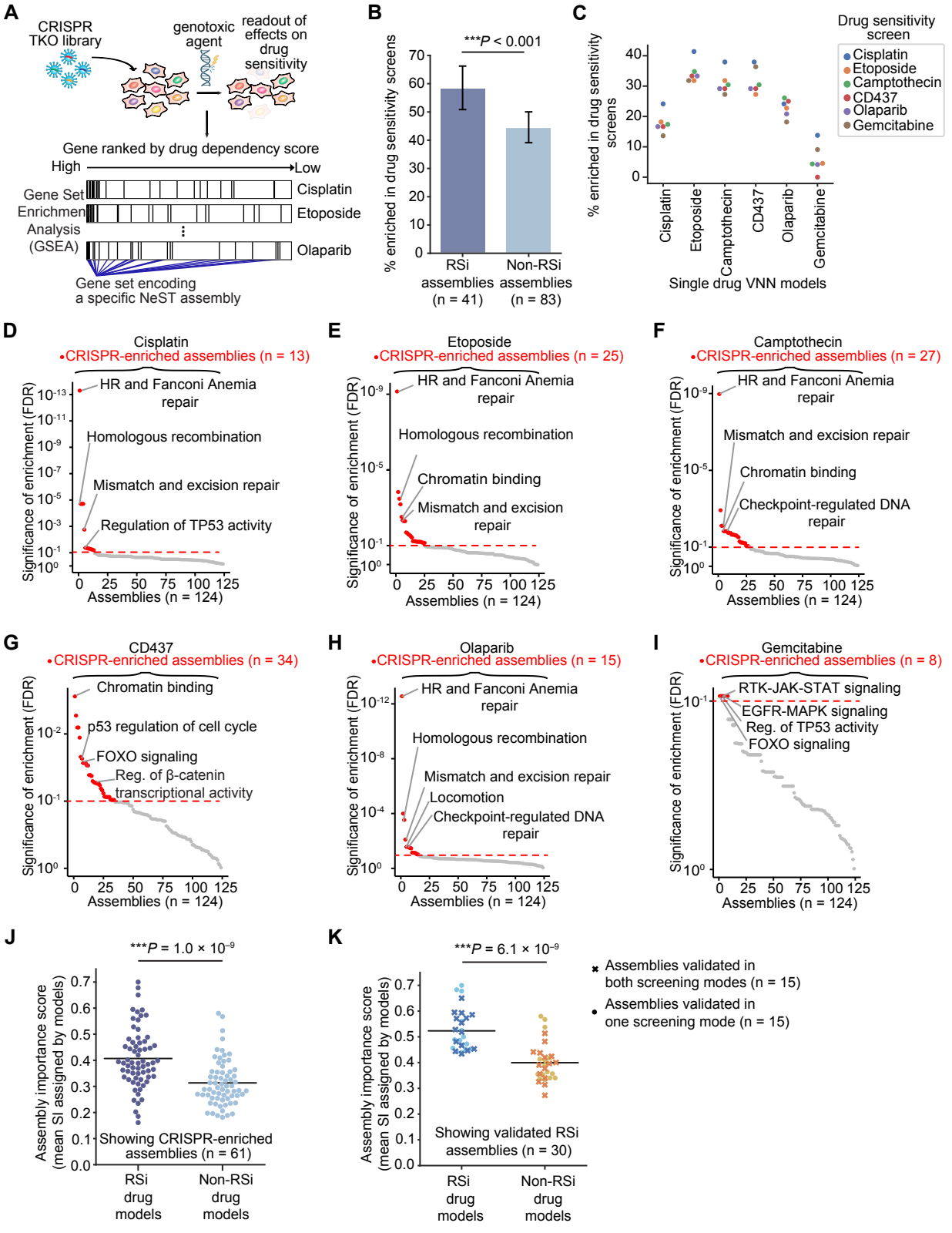

Supplementary Figure S5. Evaluation of assemblies by systematic drug sensitivity screens. **A,** Assemblies are analyzed for their enrichment for CRISPR/Cas9 gene knockouts that affect sensitivity to an RSi drug in either direction (increased or decreased sensitivity). Genetic screen and scoring by Olivieri et al. (47). **B,** Percent of assemblies enriched in drug sensitivity screens, shown separately for assemblies important to RSi drug models (left) versus all others (right). Error bars display the standard error of the proportion. ***$P < 0.01$; P-value by two sample z-test. **C,** Percent of important assemblies in single-drug VNN models enriched in each individual drug sensitivity screen. **D,** NeST assemblies ranked by their degree of enrichment in cisplatin screen, from most to least significant. Assemblies with FDR < 0.1 are highlighted in red. **E,** NeST assemblies ranked by their degree of enrichment in etoposide screen, from most to least significant. Assemblies with FDR < 0.1 are highlighted in red. **F,** NeST assemblies ranked by their degree of enrichment in camptothecin screen, from most to least significant. Assemblies with FDR < 0.1 are highlighted in red. **G,** NeST assemblies ranked by their degree of enrichment in CD437 screen, from most to least significant. Assemblies with FDR < 0.1 are highlighted in red. **H,** NeST assemblies ranked by their degree of enrichment in olaparib screen, from most to least significant. Assemblies with FDR < 0.1 are highlighted in red. **I,** NeST assemblies ranked by their degree of enrichment in gemcitabine screen, from most to least significant. Assemblies with FDR < 0.1 are highlighted in red. In panels D-I, selected RSi assemblies were labeled. **J,** Mean importance scores for assemblies enriched in one or more drug sensitivity screens (union from panels D-I, N = 61), shown separately for RSi (left) and non-RSi drug models (right). ***$P < 0.01$; P-value by Mann-Whitney U test. **K,** Mean importance scores for assemblies validated in functional screens, shown separately for RSi (left) and non-RSi drug models (right). ***$P < 0.01$; P-value by Mann-Whitney U test.

Supplementary Figure S6

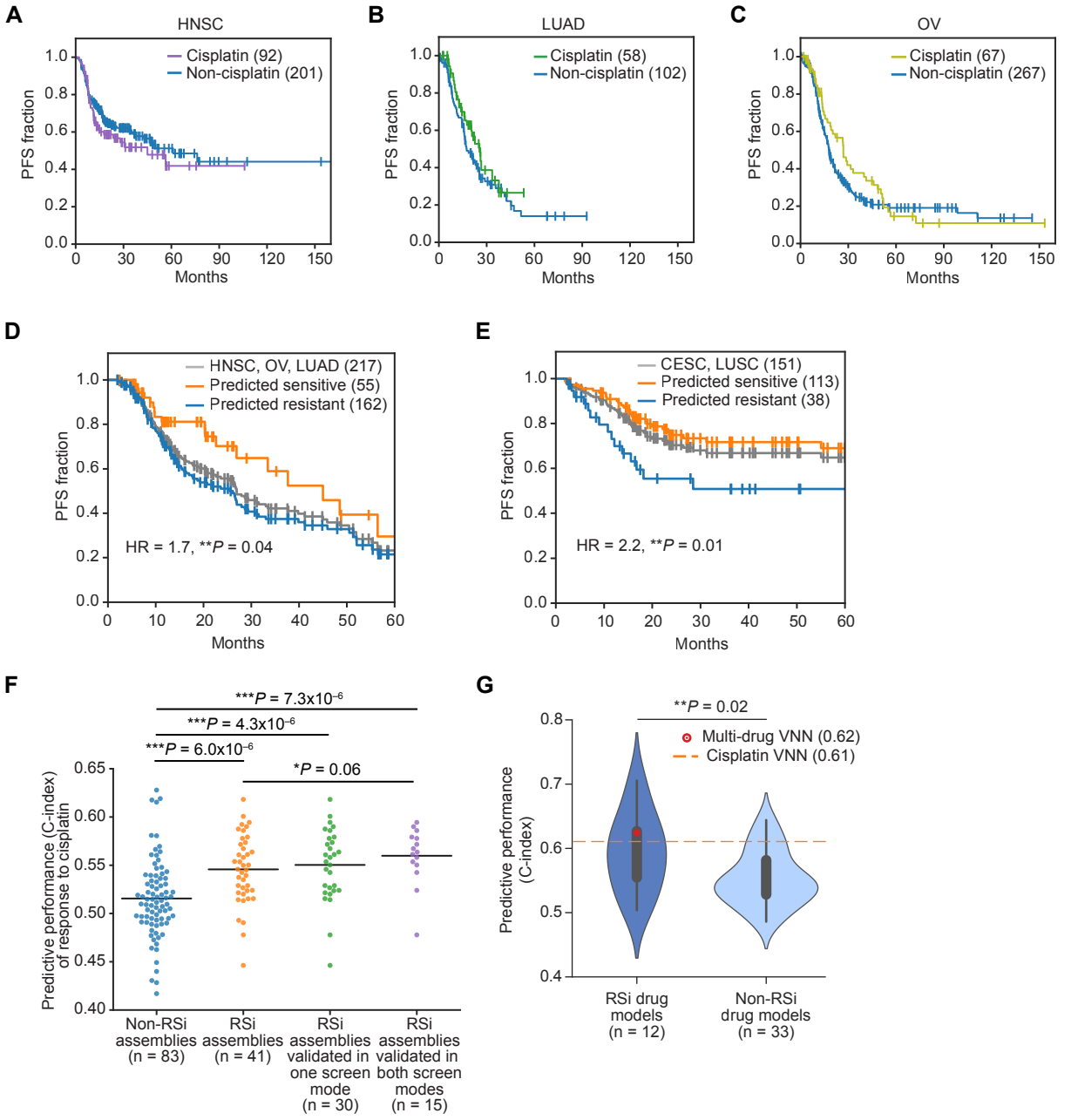

Supplementary Figure S6. Survival analysis of cisplatin-treated TCGA cohorts.
A–C, Kaplan-Meier progression-free survival (PFS) plots are shown for cisplatin-treated vs. non-cisplatin-treated patients from the TCGA head-and-neck squamous cell carcinoma (HNSC, panel A), lung adenocarcinoma (LUAD, B) and ovarian carcinoma (OV, C) cohorts. None of these panels show significant effects of cisplatin on PFS (all $P > 0.1$). **D,** Kaplan-Meier PFS plots for HNSC, OV, and LUAD patients stratified by the cisplatin VNN prediction status. **E,** Kaplan-Meier PFS plots for CESC and LUSC patients stratified by the cisplatin VNN prediction status. **F,** Swarmplot showing the predictive performance (C-index) of assemblies in response to cisplatin in patients with CESC. Assemblies are grouped into the 83 non-RSi assemblies, 41 RSi assemblies, 30 assemblies validated in at least one screening mode and 15 assemblies validated in both screening modes (from left to right). ***$P < 0.01$; *$P < 0.1$; P-value by Mann-Whitney U test. **G,** Performance comparison of 12 RSi drug models and 33 non-RSi drug models predicting response to cisplatin-treated patients with CESC. Performance measured by concordance index (C-index); **$P < 0.05$; P-value by Mann-Whitney U test. For all Kaplan-Meier plots, sensitive versus resistant shown respectively by blue versus orange; **$P < 0.05$; P-value by log-rank test.